phys. stat. sol. (a) **205**, No. 1, 96–100 (2008) / **DOI** 10.1002/pssa.200777478

physica status solidi a
www.pss-a.com
applications and materials science

Nanostructure engineering of staggered InGaN quantum wells light emitting diodes emitting at 420–510 nm

Ronald A. Arif[*], Yik-Khoon Ee, and Nelson Tansu[**]

Center for Optical Technologies, Department of Electrical and Computer Engineering, Lehigh University, 7 Asa Drive, Bethlehem, Pennsylvania 18015, USA

Received 9 July 2007, accepted 15 October 2007
Published online 15 January 2008

PACS 81.15.–z, 85.30.–z, 85.35.Be, 85.60.–q, 85.60.Bt, 85.60.Jb

[*] Corresponding author: e-mail raa4@lehigh.edu, Phone: 1-(610) 758 4326, Fax: 1-(610) 758 2605
[**] e-mail tansu@lehigh.edu, Phone: 1-(610) 758 2678, Fax: 1-(610) 758 2605

We demonstrated staggered InGaN quantum wells (QW) grown by metalorganic chemical vapor deposition (MOCVD) as improved active region for visible light emitters. Theoretical studies indicate that staggered InGaN QW with step-function like In-content in the well offers significantly improved radiative recombination rate and optical gain, in comparison to the conventional InGaN QW. Experimental results of light emitting diode (LED) structure utilizing staggered InGaN QW show good agreement with theory. Staggered InGaN QW allows polarization engineering leading to improvement of photoluminescence intensity and LEDs output power as a result of enhanced radiative recombination rate.

1 Introduction High performance visible-light emitters have found increasing use in medical, optical storage, defence, and solid-state lighting applications. Conventional III-Nitride active media for lasers and light emitting diodes (LEDs) emitting in the visible regime is based on type-I InGaN quantum wells (QWs) [1–7]. To realize high performance conventional InGaN QW LEDs and lasers, one has to overcome two major challenges, 1) the high defect density and phase segregation in high-In content InGaN QW, and 2) polarization-induced electrostatic field inherent in nitride materials. The high threading dislocation density in III-Nitrides leads to low radiative efficiency, while spontaneous and piezoelectric polarizations induce a built-in electrostatic field resulting in significant reduction of electron–hole wavefunction overlap (Γ_{e-hh}) [8–10]. The radiative recombination rate and optical gain of the QW hence will be further reduced due to this low overlap Γ_{e-hh}. These challenges lead to high threshold current densities ($J_{th} \sim 1.5–6$ kA/cm^2, $\lambda = 425–482$ nm) even in current state-of-the-art type-I InGaN QW lasers [11].

In conventional InGaN QW, the inherent spontaneous and piezoelectric polarization-induced electric field causes energy band-bending leading to quantum-confined Stark effect and spatial separation of electron and hole wavefunction in the QW. As a result, electron–hole wavefunction overlap (Γ_{e-hh}) diminishes with increasing QW thickness and higher In-content for longer wavelength emission. To illustrate the detrimental effect of the internal polarization fields on the electron–hole wavefunction overlap (Γ_{e-hh}), the emission wavelength and electron–hole wavefunction overlap (Γ_{e-hh}) of 25 Å thick type-I InGaN QW as function of In-content has been computed using our numerical model, as shown in Fig. 1. The parameters used in our numerical model are described in Section 2.2. Previously, the dependence of emission wavelength and transition matrix element on In-content in 30 Å thick InGaN QW had been shown [12]. A similar trend is also observed in our calculation result, as summarized in Fig. 1. As the In-content in the InGaN QW is increased to extend the emission wavelength, the wavefunction overlap is reduced to only 27.7% for peak emission wavelength λ_{peak} at 531.9 nm (yellow-green regime) due to the existence of large internal polarization field leading to severe charge separation effect. This reduction in Γ_{e-hh} due to polarization field is hence strongly detrimental in achieving low threshold current density lasers and high efficiency LEDs with InGaN QWs active regions, in particular for high In-content InGaN QWs. In this work, we present an approach

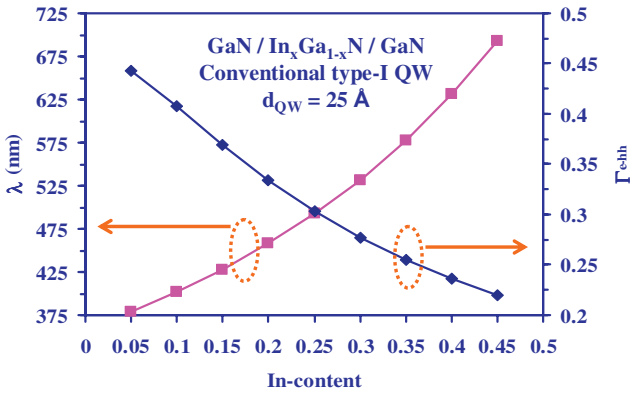

Figure 1 (online colour at: www.pss-a.com) Emission wavelength and electron–hole wavefunction overlap (Γ_{e-hh}) for 25 Å thick conventional $In_xGa_{1-x}N$ QW with GaN barriers, as function of In-content.

to improve radiative recombination rate and efficiency in nitride-based active region by utilizing staggered InGaN QW with step-function In-content profile in the QW [13].

2 Theoretical Background

2.1 Theory of Radiative Recombination Rate

According to Fermi's golden rule, the electronic transition from state $|2\rangle$ to $|1\rangle$ is governed by transition matrix element via the perturbation Hamiltonian $\hat{H}'_{21}$ [13], resulting in quantum mechanical transition rate $W_{2\to1}$ as follows

$$W_{2\to1} = \frac{2\pi}{\hbar}\cdot|H'_{21}|^2\ \rho_f(E_1 = E_2 - \hbar\omega_0)\,, \tag{1}$$

where ρ_f is the density of the final states, and $\hat{H}'_{21}$ can be expressed as a function of the transition matrix element and the envelope functions overlap. In semiconductor, the transitions occur between states in the conduction band and valence band, resulting in the following perturbation Hamiltonian

$$|H'_{21}|^2 \propto \cdot|\langle u_c|\,\hat{e}\cdot\boldsymbol{p}|u_v\rangle|^2\cdot|\langle F_2\,|\,F_1\rangle|^2\,, \tag{2}$$

which depends on the square of the transition matrix element $|M_T|^2 = |\langle u_c|\,\hat{e}\cdot\boldsymbol{p}|u_v\rangle|^2$ and the square of the envelope electron-hole wave function overlap Γ_{e-hh}. The $|u_c\rangle$ and $|u_v\rangle$ refer to the conduction and valence band Bloch functions, respectively, while the $|F_2\rangle$ and $|F_1\rangle$ are the envelope electron and hole wavefunctions, respectively. The strength of the electric field and electron interaction is indicated by the dot product of electric field polarization and the electron momentum $\boldsymbol{p}$. For the case of spontaneous recombination, the transition matrix element term reduces to $|\langle u_c\,|\,u_v\rangle|^2$ since the emission is not initiated by the presence of existing photons, but energy fluctuations in the vacuum state instead [14]. Both the spontaneous radiative recombination rate ($W_{\text{Spontaneous}}$) and stimulated emission rate ($W_{\text{Stimulated}}$) are then proportional to the square of the envelope electron and hole wavefunction overlap $|\Gamma_{e-hh}|^2$, as follows:

$$W_{\text{Spontaneous}} \sim |\langle u_c\,|\,u_v\rangle|^2\cdot|\Gamma_{e-hh}|^2\,, \tag{3}$$

$$W_{\text{Stimulated}} \sim |\langle u_c|\,\hat{e}\cdot\boldsymbol{p}|u_v\rangle|^2\cdot|\Gamma_{e-hh}|^2\,. \tag{4}$$

Therefore, radiative recombination rate and optical gain of III-Nitride active regions can be enhanced by engineering the nanostructures with improved overlap.

2.2 Numerical model development To analyze and optimize various designs of the InGaN QW structure, we have developed a numerical framework based on model solid theory utilizing Kane's model for wurtzite band edge energies and Luttinger–Kohn's model for the band structure parameters. The band parameters for the III-Nitride alloys were obtained from Refs. [15–21]. The GaN electron effective mass constants of $0.18m_0$ and $0.2m_0$ were used for the *c*-axis and transverse direction, respectively [16]. The InN electron effective mass of $0.11m_0$ was used for both the *c*-axis and transverse directions [16]. The heavy hole effective masses were calculated following the treatment presented in Ref. [18]. The ratio of conduction and valence band offsets $\Delta E_c : \Delta E_v$ is taken as 70:30 [20]. The energy gap of the InGaN QW is calculated using bowing parameter of 1.4 eV [15] and InN energy gap of 0.6405 eV [20]. Indium concentration profile along the growth axis is incorporated into energy band lineup, with the effects of strain taken into account in the form of band edge energy shifts. Polarization-induced electric field is manifested in the energy band bending. The spontaneous polarization $P_{\text{sp-InGaN}}$ (C/m^2) and piezoelectric polarization $P_{\text{pz-InGaN}}$ (C/m^2) in the InGaN QW were calculated using the following relations [21]:

$$P_{\text{sp-InGaN}}(x) = -0.042x - 0.034(1-x) + 0.037x(1-x)\,, \tag{5}$$

$$P_{\text{pz-InGaN}}(x) = 0.148x - 0.0424x(1-x)\,, \tag{6}$$

with x as the In-content in the QW. Quantum-confined energy levels of electron and hole are next computed using effective mass approximation with propagation matrix approach (step size = 0.5 Å) for multilayer heterostructures [22]. Electron–hole wavefunction overlap can then be optimized for the InGaN-based QW structures emitting at a particular wavelength regime.

3 Staggered InGaN quantum wells at 420 nm In our approach, the radiative efficiency enhancement of the InGaN-based QWs was obtained via optimizing the radiative recombination rate for the specific QW active region emitting at a particular wavelength, by using staggered InGaN QW structures. To optimize the radiative recombination rate of nitride-based active region at a particular peak wavelength, novel design of staggered InGaN quantum well with improved electron–hole wave function overlap and momentum matrix element was utilized. Figure 2(a)

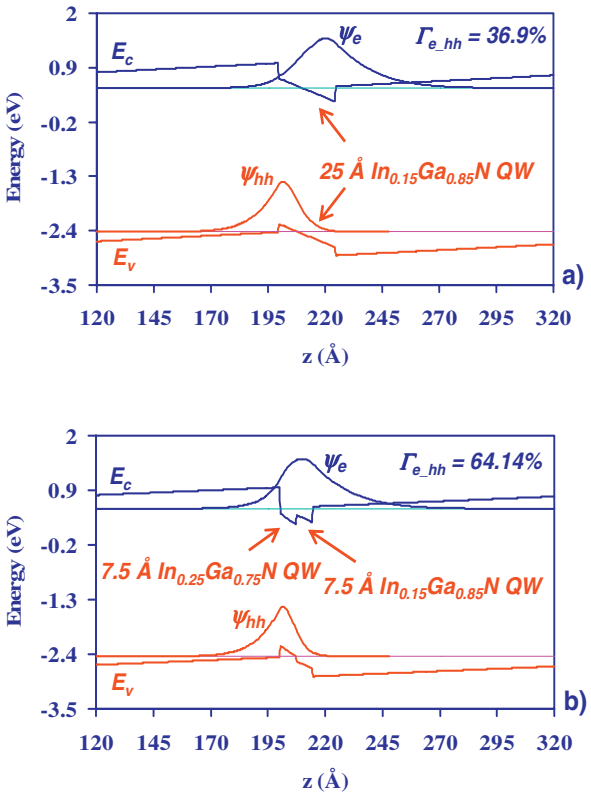

Figure 2 (online colour at: www.pss-a.com) Energy band lineups of (a) 25 Å conventional type-I $In_{0.25}Ga_{0.75}N$ QW, and (b) staggered 7.5 Å $In_{0.25}Ga_{0.75}N$/7.5 Å $In_{0.15}Ga_{0.85}N$ QW, with emission wavelengths at 420–430 nm.

shows the band lineup of 25 Å $In_{0.15}Ga_{0.85}N$ QW surrounded by GaN barriers with its corresponding electron and hole wave functions, for emission at λ_{peak} = 427.5 nm regime. The polarization fields in the conventional InGaN QW lead to low wavefunction overlap Γ_{e-hh} of only 36.9%. The staggered QW structures (designed for λ_{peak} = 421 nm) consist of 7.5 Å $In_{0.25}Ga_{0.75}N$/7.5 Å $In_{0.15}Ga_{0.85}N$ layers surrounded by GaN barriers, as shown in Fig. 2(b). The utilization of staggered InGaN QWs leads to the 'pulling' of electron wavefunction from the right to the center of the QW, due to the lighter electron effective mass in comparison to that of the hole. The hole wave function is relatively unchanged due to the heavier hole effective mass. As a result, the wavefunction overlap Γ_{e-hh} for the staggered InGaN QWs is increased to 64.14%. An improvement of the wavefunction overlap (Γ_{e-hh}) by a factor of 1.74 translates to ~3.02 times improvement in radiative recombination rate and optical gain of the active region. In our studies, the conventional and staggered InGaN QWs were designed for emission at a particular wavelength regime, with the staggered QWs designed for optimized wavefunction overlap (Γ_{e-hh}) at that regime.

4 MOCVD experiments Experiments to compare the optical properties of staggered InGaN QWs and conventional InGaN QW, with emission wavelength at 420–430 nm. Both the conventional and staggered InGaN QWs samples were grown by metalorganic chemical vapor deposition (MOCVD) on 2.5 μm thick undoped GaN (T_g = 1080 °C) grown on *c*-plane sapphire, employing a low temperature 30 nm GaN buffer layer (T_g = 535 °C). The conventional QW structure consists of 4-periods of 25 Å $In_{0.15}Ga_{0.85}N$ QW, while the staggered QW structure is formed by 4-periods of 7.5 Å $In_{0.25}Ga_{0.75}N$/7.5 Å $In_{0.15}Ga_{0.85}N$ layers. We employed 12 nm GaN barriers in both QW structures. All the active and barrier regions in the structures studied were grown at a temperature of 720 °C. The composition and growth rate of the $In_xGa_{1-x}N$ alloy were calibrated individually for a particular composition using high-resolution X-ray diffraction (XRD) measurements. The staggered InGaN QW is then realized using growth conditions (gas flows, V/III ratio, growth rate and duration, temperature, and growth pressure) obtained from this calibration. The In-content and thicknesses for QW structures are then verified by comparing the peak photoluminescence (PL) wavelengths with the data from XRD calibration and numerical model.

5 PL and CL measurements and discussions Room temperature cathodoluminescence (RT-CL) measurements were performed utilizing 10 keV electron beam with 1 μA of current over a raster scan area size of 800 × 600 μm^2, with integration time of 0.1 second. The CL emission wavelengths for staggered QW and conventional QW are measured as 407 nm and 417 nm, respectively. The CL emission of both the staggered and conventional QWs were blue-shifted by 10–15 nm in comparison to those of the PL wavelengths, presumably due to larger carrier screening effect in CL measurements. As shown in Fig. 3(a), the staggered QW structure exhibited an increase of CL peak intensity and integrated luminescence intensity by a factor of 3.37 and 4.15 times, respectively, in comparison to those of the conventional QW.

Room temperature photoluminescence (RT-PL) measurements were also performed on both samples using 325 nm He–Cd lasers. Referring to Fig. 3(b), the PL peak emission wavelengths (λ_{peak}) of the staggered QW and conventional QW were measured as 416 nm and 433 nm, respectively. The peak PL and integrated PL luminescence intensities for the staggered $In_{0.25}Ga_{0.75}N$/$In_{0.15}Ga_{0.85}N$ QWs exhibited improvement by a factor of 4.74 times and 4.39 times, respectively, in comparison to those of the conventional $In_{0.25}Ga_{0.75}N$ QW. It is also important to point out that integrated luminescence improvement in the staggered InGaN QW is not accompanied by increased linewidth, rather it is attributed to higher peak intensity at the same excitation laser power. This is consistent with the fact that the measurements were conducted at the same temperature employing identical optical excitation power to facilitate direct spectrum comparison. The PL full width at half max (FWHM) for staggered InGaN QWs is measured as 14.8 nm (106.2 meV), which is comparable to that of the conventional InGaN QW (FWHM = 17.26 nm or

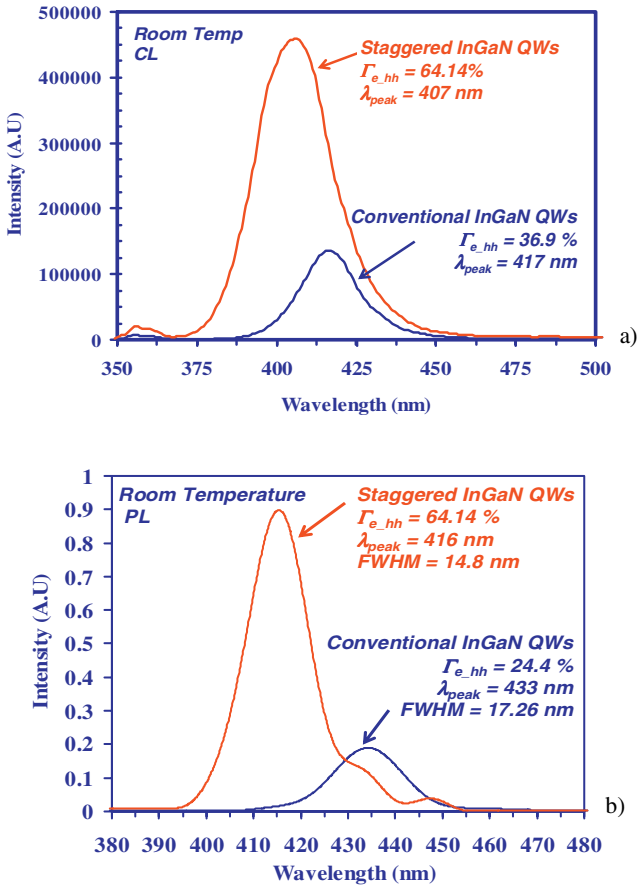

Figure 3 (online colour at: www.pss-a.com) Room-temperature a) CL spectra and b) PL spectra of staggered 7.5 Å $In_{0.25}Ga_{0.75}N$/7.5 Å $In_{0.15}Ga_{0.85}N$ QW and 25 Å conventional type-I $In_{0.25}Ga_{0.75}N$ QW.

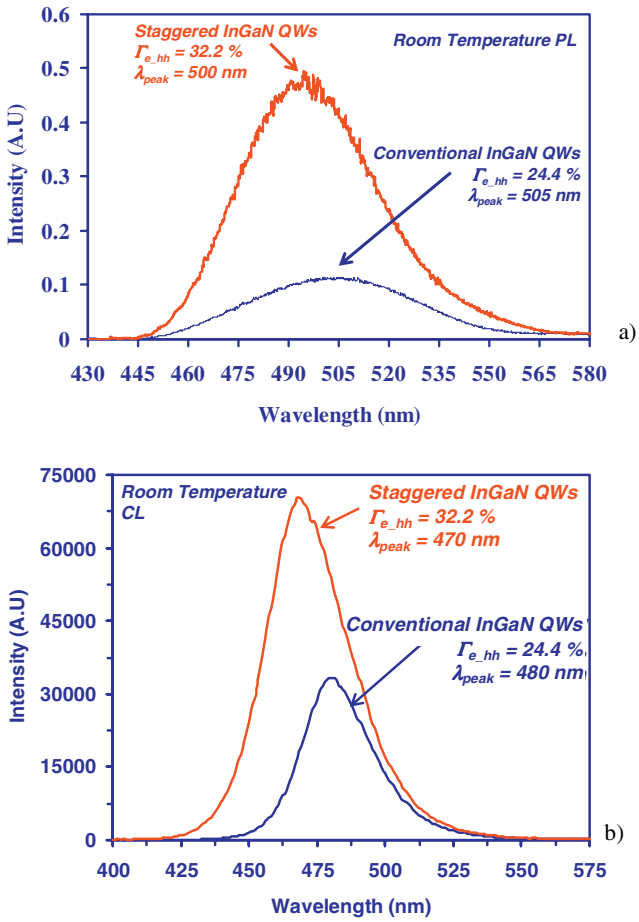

Figure 4 (online colour at: www.pss-a.com) Room-temperature a) PL spectra and b) CL spectra of of staggered 13 Å $In_{0.28}Ga_{0.72}N$/13 Å $In_{0.21}Ga_{0.79}N$ QW and 27 Å conventional $In_{0.26}Ga_{0.74}N$ QW.

113.8 meV). The comparable PL FWHMs indicate that the material qualities of both the staggered and conventional InGaN QWs are similar.

6 Staggered InGaN quantum wells at 500 nm

To further extend the concept of staggered InGaN QW emitting at longer wavelength, we conducted experiments utilizing 27 Å conventional $In_{0.26}Ga_{0.74}N$ QW ($\Gamma_{e-hh} = 24.4\%$) and staggered 13 Å $In_{0.28}Ga_{0.72}N$/13 Å $In_{0.21}Ga_{0.79}N$ QW ($\Gamma_{e-hh} = 32.2\%$), emitting at $\lambda_{peak} = 500-515$ nm. As shown in Fig. 4(a), the staggered $In_{0.28}Ga_{0.72}N/In_{0.21}Ga_{0.79}N$ QW exhibited improvements in the peak PL and the total integrated PL luminescence intensity by 4.48 and 3.54 times, respectively. Referring to Fig. 4(b), the staggered QW structure exhibited an increase of CL peak intensity and integrated luminescence intensity by a factor of 2.1 and 2.43 times, respectively, in comparison to those of the conventional QW. The PL and CL improvements were higher than what were predicted from the increase in overlap (Γ_{e-hh}) alone. The improvements can thus be presumably due to (1) better materials quality in staggered InGaN QW, and (2) lower 'effective' QW thickness in the staggered QW structure – as compared to that of the conventional InGaN QW – leading to higher carrier concentration in the QW and higher radiative efficiency, hence further enhancing the intensity improvement.

7 LEDs device characteristics To assess the staggered QWs for device applications, we realized two LED structures ($\lambda_{peak} = 455-465$ nm) utilizing (1) 4-periods of staggered QWs of 12 Å $In_{0.25}Ga_{0.75}N$/12 Å $In_{0.15}Ga_{0.85}N$ layers ($\Gamma_{e-hh} = 43.1\%$), and (2) 4-periods of 27 Å conventional $In_{0.21}Ga_{0.79}N$ QW ($\Gamma_{e-hh} = 27.4\%$) as the active regions of each LED. Both structures were grown on 2.5 µm n-GaN template ($n = 3 \times 10^{18}$ cm^{-3}) on *c*-plane sapphire substrates. The acceptor level for the p-GaN layer is 3×10^{17} cm^{-3}.

Finally, we also evaluated the performance of our staggered InGaN QW active region in LEDs by performing continuous wave (CW) power measurements at room temperature. Figure 5 shows that the output power is linear as function of driving current up to 100 mA for both LEDs with area of 1 mm^2. Staggered QW LEDs exhibited an improvement in output power by 11.2 times at current level

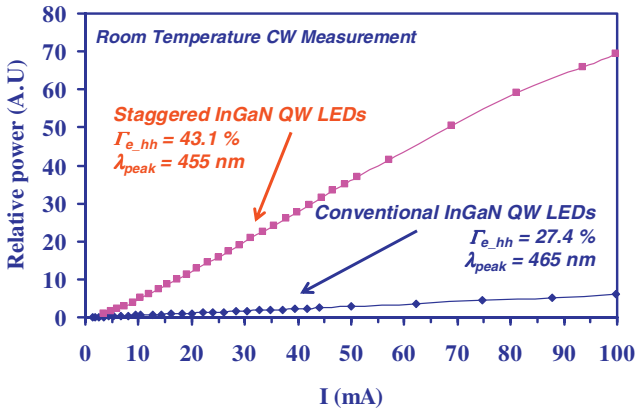

Figure 5 (online colour at: www.pss-a.com) Relative light output power versus injected current for staggered 12 Å $In_{0.25}Ga_{0.75}N$/12 Å $In_{0.15}Ga_{0.85}N$ QWs LED and 27 Å conventional $In_{0.21}Ga_{0.79}N$ QW LED.

of 100 mA. The measured significant enhancement is larger than that predicted theoretically, and several possible factors may contribute to this improvement, such as: (1) more pronounced carrier screening reduces energy band-bending and further increases Γ_{e-hh} of the staggered InGaN QWs, (2) improved material quality of the staggered InGaN QWs, and (3) better carrier confinement in the staggered InGaN QWs. Further studies and optimizations are still required to elucidate more insights into the physics of polarization engineering of nitride-based active regions, in particular recombination analysis and structural analysis of the staggered InGaN QW are needed to clarify the factors leading to this improvement.

8 Conclusion Nanostructure engineering for minimizing the detrimental impact of polarization-induced electric field using staggered InGaN QWs has been demonstrated. In good agreement with theory, increased wavefunction overlap (Γ_{e-hh}) leading to significant enhancement of radiative recombination rate is evident in improved PL peak and integrated luminescence by a factor of 4.74 times and 4.39 times (and 4.48 times and 3.54 times), respectively, for staggered InGaN QWs active regions emitting at $\lambda_{peak} = 420-430$ nm (and $\lambda_{peak} = 500-505$ nm). Preliminary LEDs device had also been fabricated utilizing staggered InGaN QW emitting at $\lambda_{peak} = 455-465$ nm, resulting in almost an order of magnitude improvement in the output power of the devices. The use of polarization control for enhancing the Γ_{e-hh} of the InGaN-based active regions can hence be potentially applicable for high-efficiency LEDs and low-threshold nitride-based lasers.

Acknowledgements The authors would like to acknowledge funding supports from US Department of Defense – Army Research Lab, National Science Foundation (NSF) Award #0701421, and Peter C. Rossin Assistant Professorship Funds.

References

[1] S. Nakamura, M. Senoh, N. Iwasa, S. Nagahama, T. Yamada, and T. Mukai, Jpn. J. Appl. Phys. **34**, L1332 (1995).
[2] S. Nakamura, M. Senoh, S. Nagahama, N. Iwasa, T. Yamada, T. Matshushita, H. Kiyoku, and Y. Sugimoto, Jpn. J. Appl. Phys. **35**, L74 (1996).
[3] S. Chhajed, Y. Xi, Y.-L. Li, Th. Gessmann, and E. F. Schubert, J. Appl. Phys. **97**, 054506 (2005).
[4] W. Zhao, Y. Li, T. Detchprohm, and C. Wetzel, phys. stat. sol. (c) **4**, 9 (2007).
[5] R. H. Horng, C. C. Yang, J. Y. Wu, S. H. Huang, C. E. Lee, and D. S. Wuu, Appl. Phys. Lett. **86**, 221101 (2005).
[6] J. S. Cabalu, A. D. Williams, T. C. P. Chen, R. France, and T. D. Moustakas, in: Proceedings of Materials Research Society Fall Meeting, Boston, MA, USA 2005, p. 892.
[7] J. Zhang, J. Yang, G. Simin, M. Shatalov, M. Asif Khan, M. S. Shur, and R. Gaska, Appl. Phys. Lett. **77**, 2668 (2000).
[8] T. Deguchi, K. Sekiguchi, A. Nakamura, T. Sota, R. Matsuo, S. Chichibu, and S. Nakamura, Jpn. J. Appl. Phys. **38**, L914 (1999).
[9] F. Bernardini, V. Fiorentini, and D. Vanderbilt, Phys. Rev. B **56**, R10024 (1997).
[10] F. Bernardini and V. Fiorentini, Phys. Rev. B **57**, R9427 (1998).
[11] S. Nagahama, Y. Sugimoto, T. Kozaki, and T. Mukai, in: Proceedings of SPIE Photonics, West, San Jose, CA, USA 2005.
[12] C. Wetzel, S. Kamiyama, H. Amano, and I. Akasaki, Jpn. J. Appl. Phys. **41**, 11 (2002).
[13] R. A. Arif, Y.-K. Ee, and N. Tansu, Appl. Phys. Lett. **91**, 091110 (2007).
[14] J. Singh, Electronic and Optoelectronic Properties of Semiconductor Structures (Cambridge University Press, 2003).
[15] I. Vurgaftman and J. R. Meyer, J. Appl. Phys. **94**, 3675 (2003).
[16] J. Piprek, Semiconductor Optoelectronic Devices: Introduction to Physics and Simulation (Academic Press, London, 2003).
[17] S. L. Chuang, IEEE J. Quantum Electron. **32**, 1791 (1996).
[18] S. L. Chuang and C. S. Chang, Phys. Rev. B **54**, 2491 (1996).
[19] Y. C. Yeo, T. C. Chong, M. F. Li, and W. J. Fan, J. Appl. Phys. **84**, 1813 (1998).
[20] J. Wu, W. Walukiewicz, W. Shan, K. M. Yu, J. W. Ager III, S. X. Li, E. E. Haller, H. Lu, and W. J. Schaff, J. Appl. Phys. **94**, 4457 (2003).
[21] O. Ambacher, J. Majewski, C. Miskys, A. Link, M. Hermann, M. Eickhoff, M. Stutzmann, F. Bernardini, V. Fiorentini, V. Tilak, W. J. Schaff, and L. F. Eastman, J. Phys.: Condens. Matter **14**, 3399 (2002).
[22] S. L. Chuang, Physics of Optoelectronic Devices (John Wiley and Sons, New York, 1995).

